CMB ANISOTROPIES AND THE DETERMINATION OF COSMOLOGICAL PARAMETERS

G EFSTATHIOU
Institute of Astronomy
Madingley Road
Cambridge CB3 OHA

1. Abstract

I review the basic theory of the cosmic microwave background (CMB) anisotropies in adiabatic cold dark matter (CDM) cosmologies. The latest observational results on the CMB power spectrum are consistent with the simplest inflationary models and indicate that the Universe is close to spatially flat with a nearly scale invariant fluctuation spectrum. We are also beginning to see interesting constraints on the density of CDM, with a best fit value of $\omega_c \equiv \Omega_c h^2 \sim 0.1$. The CMB constraints, when combined with observations of distant Type Ia supernovae, are converging on a Λ-dominated Universe with $\Omega_m \approx 0.3$ and $\Omega_\Lambda \approx 0.7$.[1]

2. Introduction

The discovery of temperature anisotropies in the CMB by the COBE team (Smoot *et al.* 1992) heralded a new era in cosmology. For the first time COBE provided a clear detection of the primordial fluctuations responsible for the formation of structure in the Universe at a time when they were still in the linear growth regime. Since then, a large number of ground based and balloon borne experiments have been performed which have succeeded in defining the shape of the power spectrum of temperature anisotropies C_ℓ[2] up to multipoles of $\ell \sim 300$ clearly defining the first acoustic peak in the spectrum. Figure 1 shows a compilation of band power anisotropy

[1]To appear in Proceedings of NATO ASI: Structure formation in the Universe, eds. N. Turok, R. Crittenden.

[2]The power spectrum is defined as $C_\ell = \langle |a_{\ell m}|^2 \rangle$, where the $a_{\ell m}$ are determined from a spherical harmonic expansion of the temperature anisotropies on the sky, $\Delta T/T = \sum a_{\ell m} Y_{\ell m}(\theta, \phi)$.

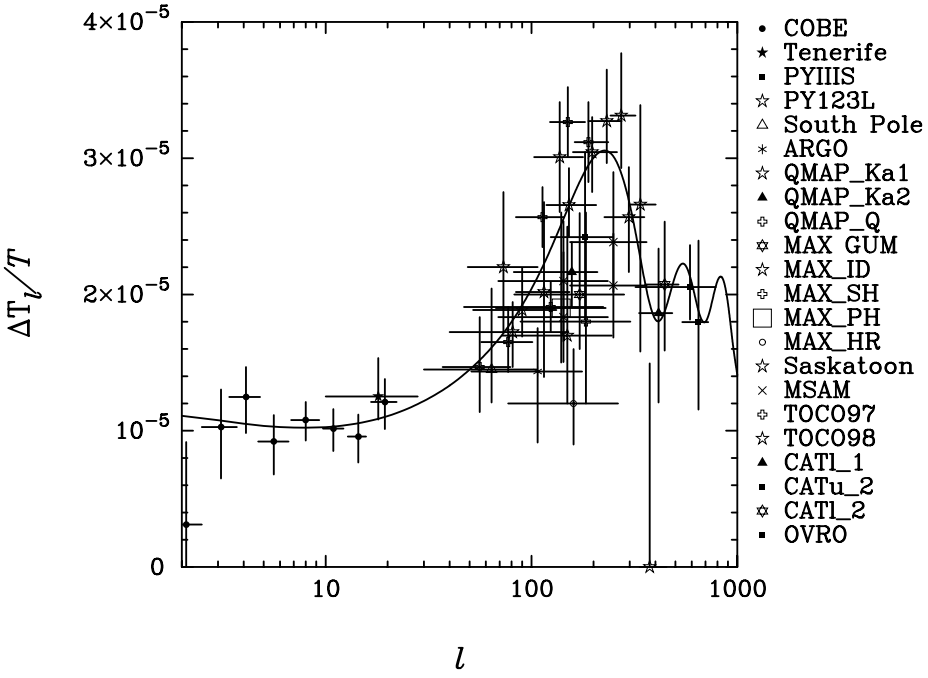

Figure 1. Current constraints on the power spectrum of CMB temperature anisotropies. The error bars in the vertical direction show 1σ errors in the band power estimates and the error bars in the horizontal direction indicate the width of the band. The solid line shows the best fit adiabatic CDM model with parameters $\omega_b = 0.019$, $\omega_c = 0.10$, $n_s = 1.08$, $Q_{10} = 0.98$, $\Omega_m = 0.225$, $\Omega_\Lambda = 0.775$.

measurements

$$\frac{\Delta T_\ell}{T} = \sqrt{\frac{1}{2\pi}\ell(\ell+1)C_\ell} \tag{1}$$

that is almost up to date at the time of writing. The horizontal error bars show the multipole range probed by each experiment. The recent results from the VIPER experiment (Peterson *et al.* 1999) and the Boomerang test flight (Mauskopf *et al.* 1999) are not plotted because the exact window functions are not yet publically available. Neither are the published results from the Python V experiment (Coble *et al.* 1999) which seem to be discrepant with the other experiments particularly in the multipole range $\ell \lesssim 100$. The points plotted in figure 1 are generally consistent with each other and provide strong evidence for a peak in the power spectrum at $\ell \sim 200$.

In this introductory article, I will review briefly the theory of CMB anisotropies in adiabatic models of structure formation and then discuss the implications of Figure 1 for values of cosmological parameters. The

literature on the CMB anisotropies has grown enormously over the last few years and it is impossible to do the subject justice in a short article. General reviews of the CMB anisotropies are given by Bond (1996) and Kamionkowski and Kosowsky (1999). A recent review on constraining cosmological parameters from the CMB is given by Rocha (1999).

3. Basic Theory

Most of the key features of figure 1 can be understood using a simplified set of equations. The background universe is assumed to be spatially flat together with small perturbations h_{ij} so that the metric is

$$ds^2 = a^2(\tau)\left(\eta_{ij} + h_{ij}\right) dx^i dx^j, \tag{2}$$
$$\eta_{ij} = (1,\ -1,\ -1,\ -1), \qquad \tau = \int dt/a.$$

We adopt the synchronous gauge, $h_{00} = h_{0i} = 0$, and ignore the anisotropy of Thomson scattering and perturbations in the relativistic neutrino component. With these assumptions, the equations governing the evolution of scalar plane wave perturbations of wavenumber k are

$$\dot{\Delta} + ik\mu\Delta + \Phi = \sigma_T n_e a\left[\Delta_0 + 4\mu v_b - \Delta\right] \tag{3a}$$
$$\Phi = -(3\mu^2 - 1)\dot{h}_{33} - (1-\mu^2)\dot{h} \tag{3b}$$
$$\dot{v}_b + \frac{\dot{a}}{a}v_b = \sigma_T n_e a \frac{\bar{\rho}_\gamma}{\bar{\rho}_b}\left(\Delta_1 - \frac{4}{3}v_b\right), \tag{3c}$$
$$\dot{\delta}_b = \frac{1}{2}\dot{h} - ikv_b, \qquad \dot{\delta}_C = \frac{1}{2}\dot{h} \tag{3d}$$
$$\ddot{h} + \frac{\dot{a}}{a}\dot{h} = 8\pi G a^2(\bar{\rho}_b\delta_b + \bar{\rho}_c\delta_c + 2\bar{\rho}_\gamma\Delta_0) \tag{3e}$$
$$ik(\dot{h}_{33} - \dot{h}) = 16\pi G a^2(\bar{\rho}_b v_b + \bar{\rho}_\gamma\Delta_1). \tag{3f}$$

Here, Δ is the perturbation to the photon radiation brightness and Δ_0 and Δ_1 are its zeroth and first angular moments, δ_b and δ_c are the density perturbations in the baryonic and CDM components, v_b is the baryon velocity and $h = \mathrm{Tr}(h_{ij})$. Dots denote differentiation with respect to the conformal time variable τ. It is instructive to look at the solutions to these equations in the limits of large ($k\tau_R \ll 1$) and small ($k\tau_R \gg 1$) perturbations, where τ_R is the conformal time at recombination:

3.1. LARGE ANGLE ANISOTROPIES

In the limit $k\tau_R \ll 1$, Thomson scattering is unimportant and so the term in square brackets in the Boltzmann equation for the photons can be ignored.

In the matter dominated era $h_{33} = h \propto \tau^2$ and so equation (3a) becomes

$$\dot{\Delta} + ik\mu\Delta = 2\mu^2\dot{h} \tag{4}$$

with approximate solution

$$\Delta(k,\mu,\tau) \approx -\frac{2\ddot{h}(\tau_R)}{k^2}\exp\left(ik\mu(\tau_s - \tau)\right). \tag{5}$$

This solution is the Sachs-Wolfe (1967) effect. Any deviation from the evolution $\ddot{h}$ = constant, caused for example by a non-zero cosmological constant, will lead to additional terms in equation (5) increasing the large-angle anisotropies (sometimes referred to as the late-time Sachs-Wolfe effect, see *e.g.* Bond 1996). The CMB power spectrum is given by

$$C_\ell = \frac{1}{8\pi}\int_0^\infty |\triangle_\ell|^2 k^2 dk, \tag{6}$$

where the perturbation Δ has been expanded in Legendre polynomials,

$$\Delta = \sum_\ell (2\ell+1)\Delta_\ell P_\ell(\mu). \tag{7}$$

Inserting the solution of equation (5) into equation (6) gives

$$C_\ell = \frac{1}{2\pi}\int_0^\infty \frac{|\ddot{h}|^2}{k^4} j_l^2(k\tau_0)k^2\, dk, \tag{8}$$

and so for a power-law spectrum of scalar perturbations, $|h|^2 \propto k^{n_s}$, the CMB power spectrum is

$$C_\ell = C_2 \frac{\Gamma\left(\ell + \frac{(n_s-1)}{2}\right)}{\Gamma\left(\ell + \frac{(5-n_s)}{2}\right)} \frac{\Gamma\left(\frac{9-n_s}{2}\right)}{\Gamma\left(\frac{3+n_s}{2}\right)} \tag{9}$$

giving the characteristic power-law like form, $C_\ell \propto \ell^{(n_s-3)}$ at low multipoles ($\ell \lesssim 30$).

3.2. SMALL ANGLE ANISOTROPIES AND ACOUSTIC PEAKS

In the matter dominated era, equation (3a) becomes

$$\dot{\Delta} + ik\mu\triangle = \sigma_T n_e a\left[\Delta_0 + 4\mu v_b - \Delta\right] + 2\mu^2\dot{h}, \tag{10}$$

and taking the zeroth and first angular moments gives

$$\dot{\Delta}_0 + ik\Delta_1 = \frac{2}{3}\dot{h} \tag{11a}$$

$$\dot{\Delta}_1 + ik\left(\frac{\Delta_0 + 2\Delta_2}{3}\right) = \sigma_T n_e a\left[\frac{4}{3}v_b - \Delta_1\right]. \tag{11b}$$

Prior to recombination, $\tau/\tau_c \gg 1$ where $\tau_c = 1/(\sigma_T n_e a)$ is the mean collision time, and so the matter is tightly coupled to the radiation. In this limit $\Delta_1 \approx 4/3 v_b$ from equation (3c) and Δ_2 in equation (11b) can be ignored. With these approximations, equation (11b) becomes

$$\dot{\Delta}_1 + \frac{ik\Delta_0}{3} = -\frac{\bar{\rho}_b}{\bar{\rho}_\gamma}\left[\frac{3}{4}\dot{\Delta}_1 + \frac{\dot{a}}{a}\Delta_1\right]. \tag{12}$$

Neglecting the expansion of the universe, equations (11a) and (12) can be combined to give a forced oscillator equation

$$\ddot{\Delta}_0 = -\frac{k^2}{3R}\Delta_0 + \frac{2}{3}\ddot{h}, \qquad R \equiv 1 + \frac{3\bar{\rho}_b}{4\bar{\rho}_\gamma}, \tag{13}$$

with solution

$$\Delta_0(\tau) = \left(\Delta_0(0) - \frac{2R\ddot{h}}{k^2}\right)\cos\frac{k\tau}{\sqrt{3R}} + \frac{\sqrt{3R}}{k}\dot{\Delta}_0(0)\sin\frac{k\tau}{\sqrt{3R}} + \frac{2R\ddot{h}}{k^2}, \tag{14}$$

where $\Delta_0(0)$ and $\dot{\Delta}_0(0)$ are evaluated when the wave first crosses the Hubble radius, $k\tau \sim 1$. For adiabatic perturbations the first term dominates over the second because the perturbation breaks at $k\tau \sim 1$ with $\dot{\Delta}_0 \approx 0$. It is useful to define (gauge-invariant) radiation perturbation variables

$$\tilde{\Delta}_0 = \Delta_0 - \frac{2\ddot{h}}{k^2}, \qquad \tilde{\Delta}_1 = \Delta_1 + i\frac{2\dot{h}}{3k},$$

then the solution of equation (10) is

$$\tilde{\Delta}(k,\mu,\tau) = \int_0^\tau \sigma_T n_e a\left[\tilde{\Delta}_0 + 4\mu\left(v_b + \frac{i\dot{h}}{2k}\right)\right] e^{ik\mu(\tau'-\tau) - \int_{\tau'}^{\tau}[\sigma_T n_e a]d\tau''} d\tau'. \tag{15}$$

If $k\tau \gg 1$, the second term in the square brackets is smaller than the first by a factor of $k\tau$, and the solution of equation (15) gives a power spectrum with a series of modulated acoustic peaks spaced at regular intervals of $k_m r_s(a_r) = m\pi$, where r_s is the sound horizon at recombination

$$r_s = \frac{c}{\sqrt{3}H_0\Omega_m^{1/2}}\int_0^{a_r}\frac{da}{(a+a_{equ})^{1/2}}\frac{1}{R^{1/2}}, \tag{16}$$

(Hu and Sugiyama 1995). Here a_{equ} is the scale factor when matter and radiation have equal densities and a_r is the scale factor at recombination.

The multipole locations of the acoustic peaks in the angular power spectrum are given by

$$\ell_m = \alpha m\pi\frac{d_A(z_r)}{r_s} \tag{17}$$

where α is a number of order unity and d_A is the angular diameter distance to last scattering

$$d_A = \frac{c}{H_0|\Omega_k|^{1/2}} \sin_k(|\Omega_k|^{1/2} x) \tag{18a}$$

$$x \approx \int_{a_r}^{1} \frac{da}{[\Omega_m a + \Omega_k a^2 + \Omega_\Lambda a^4]^{1/2}} \tag{18b}$$

where $\Omega_k = 1 - \Omega_\Lambda - \Omega_m$ and $\sin_k \equiv \sinh$ if $\Omega_k > 0$ and $\sin_k = \sin$ if $\Omega_k < 0$.

The general dependence of the CMB power spectrum on cosmological parameters is therefore clear. The positions of the acoustic peaks depend on the geometry of the Universe via the angular diameter distance of equation (18) and on the value of the sound horizon r_s. The relative amplitudes of the peaks depend on the physical densities of the various constituents $\omega_b \equiv \Omega_b h^2$, $\omega_c \equiv \Omega_c h^2$, $\omega_\nu \equiv \Omega_\nu h^2$, *etc.* and on the scalar fluctuation spectrum (parameterized here by a constant spectral index n_s). Clearly, models with the same initial fluctuation spectra and identical physical matter densities ω_i will have identical CMB power spectra at high multipoles if they have the same angular diameter distance to the last scattering surface. This leads to a strong *geometrical degeneracy* between Ω_m and Ω_Λ (*e.g.* Efstathiou and Bond 1999 and references therein). The power spectrum on large angular scales (equation 9) is sensitive to the spectral index and amplitude of the power spectrum, geometry of the Universe and, for extreme values of Ω_k can break the geometrical degeneracy via the late-time Sachs-Wolfe effect. We will discuss briefly some of the constraints on cosmological parameters from the current CMB data in the next section. Before moving on to this topic, I mention some important points that cannot be covered in detail because of space limitations:

• Inflationary models can give rise to tensor perturbations with a characteristic spectrum that declines sharply at $\ell \gtrsim 100$ (see *e.g.* Bond 1996 and references therein). In power-law like inflation, the tensor spectral index n_t is closely linked to the scalar spectral index, $n_t \approx n_s - 1$, and to the relative amplitude of the tensor and scalar perturbations.

• The anisotropy of Thomson scattering causes the CMB anisotropies to be linearly polarized at the level of a few percent (see Bond 1996, Hu and White 1997, and references therein). Measurements of the linear polarization can distinguish between tensor and scalar perturbations and can constrain the epoch of reionization of the intergalactic medium (Zaldarriaga, Spergel and Seljak 1997).

• The main effect of reionization is to depress the amplitude of the power spectrum at high multipoles by a factor of $\exp(-2\tau_{opt})$ where τ_{opt} is the optical depth to Thomson scattering. In the 'best fit' CDM universe described in the next section ($\omega_b = 0.019$, $h = 0.65$, $\Omega_m = \Omega_c + \Omega_b \approx 0.3$

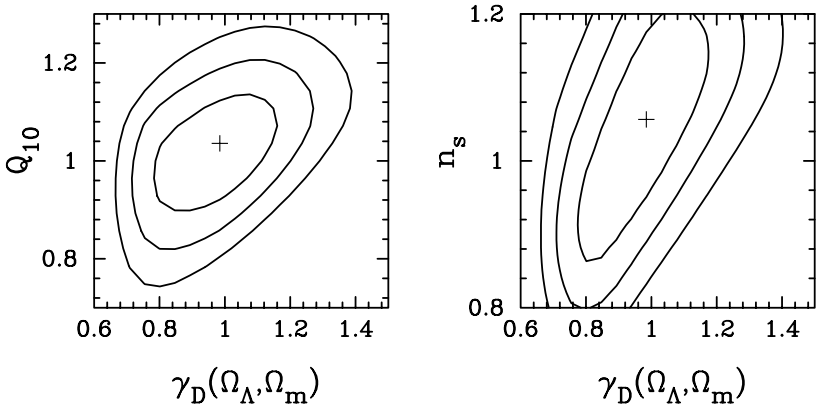

Figure 2. Marginalized likelihoods (1, 2 and 3σ contours) in the Q_{10}–γ_D and n_s–γ_D planes, where γ_D is the acoustic peak location parameter defined in equation 18.

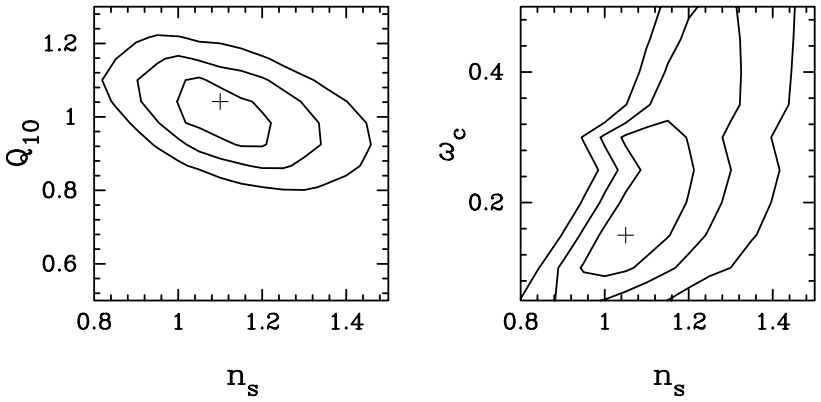

Figure 3. Marginalized likelihoods (1, 2 and 3σ contours) in the Q_{10}–n_s and ω_c–n_s planes. The crosses show where the likelihood function peaks.

and $\Omega_\Lambda \approx 0.7$) and a reionization redshift of $z_{reion} \approx 20$ (a plausible value) $\tau_{opt} \approx 0.2$ which is significant. There is a reasonable chance that we might learn something about the 'dark ages' of cosmic history from precision measurements of the CMB.

4. Cosmological Parameters from the CMB

In this section, we review some of the constraints on cosmological parameters from the CMB data plotted in figure 1. The analysis is similar to that presented in Efstathiou *et al.* (1999, hereafter E99), in which we map the full likelihood function in 5 parameters Ω_Λ, Ω_m, ω_c, n_s and Q_{10} (the amplitude of $\sqrt{C_\ell}$ at $\ell = 10$ relative to that inferred from COBE). The baryon density is constrained to $\omega_b = 0.019$, as determined from primor-

dial nucleosynthesis and deuterium abundances measurements from quasar spectra (Burles and Tytler 1998). The results presented below are insensitive to modest variations ($\sim 25\%$) of ω_b and illustrate the main features of cosmological parameter estimation from the CMB. Recently, Tegmark and Zaldarriaga (2000) have performed a heroic 10 parameter fit to the CMB data, including a tensor contribution and finite optical depth from reionization. I will discuss the effects of widening the parameter space briefly below but refer the reader to Tegmark and Zaldarriaga for a detailed analysis.

The best fit model in this five parameter space is plotted as the solid line in figure 1. It is encouraging that the best fitting model has perfectly reasonable parameters, a spatially flat universe with a nearly scale invariant fluctuation spectrum and a low CDM density $\omega_c \sim 0.1$. Marginalised likelihood functions are plotted in various projections in the parameter space in figures 2, 3 and 5 (uniform priors are assumed in computing the marginalized likelihoods, as described in E99). Figure 2 shows constraints on the position of the first acoustic peak measured by the 'location' parameter

$$\gamma_D = \frac{\ell_D(\Omega_\Lambda, \Omega_m)}{\ell_D(\Omega_\Lambda = 0, \Omega_m = 1)}, \tag{19}$$

i.e. the parameter γ_D measures the location of the acoustic peak relative to that in a spatially flat model with zero cosmological constant. The geometrical degeneracy between Ω_m and Ω_Λ described in the previous section is expressed by $\gamma_D =$ constant. Figure 2 shows that the best fitting value is $\gamma_D = 1$ with a 2σ range of about ± 0.3. The position of the first acoustic peak in the CMB data thus provides powerful evidence that the Universe is close to spatially flat.

Figure 3 shows the marginalized likelihoods in the $Q_{10} - n_s$ and $\omega_c - n_s$ planes. The constraints on Q_{10} and n_s are not very different to those from the analysis of COBE alone (see *e.g.* Bond 1996). The experiments at higher multipoles are so degenerate with variations in other cosmological parameters that they do not help tighten the constraints on Q_{10} and n_s. The constraints on ω_c and n_s show an interesting result; if $n_s \approx 1$, then the best fit value of ω_c is about 0.1 with a 2σ upper limit of about 0.3. This constraint on ω_c comes from the height of the first acoustic peak, as shown in figure 4. In this diagram, the CMB data points have been averaged in 10 band-power estimates as described by Bond, Knox and Jaffe (1998). The solid curve shows the best-fit model as plotted in figure 1, which has $\omega_c = 0.1$. The dashed lines show models with $\omega_c = 0.25$ and $\omega_c = 0.05$ with the other parameters held fixed. Raising ω_c lowers the height of the peak and vice-versa. This result is not very sensitive to variations of ω_b in the neighbourhood of $\omega_b \sim 0.02$. Reionization and the addition of a tensor component can lower the height of the first peak relative to the anisotropies

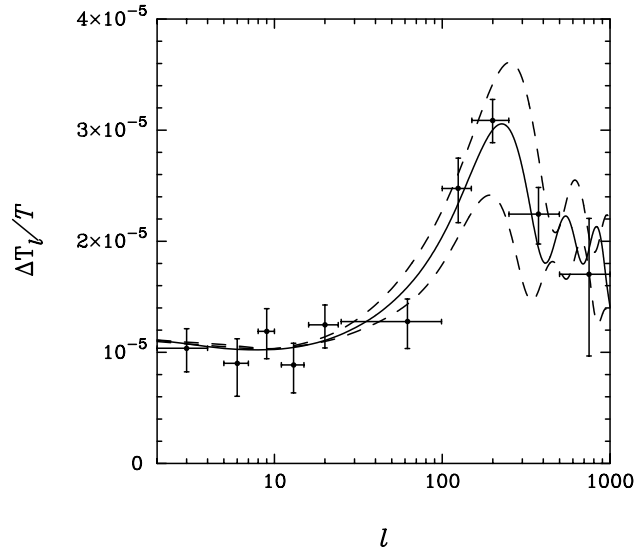

Figure 4. The crosses show maximum likelihood bandpower averages of the observations shown in figure 1 together with 1σ errors. The solid line shows the best fit adiabatic CDM model as plotted in figure 1 which has $\omega_c = 0.1$. The dashed lines show the effects of varying ω_c keeping the other parameters fixed. The upper dotted line shows $\omega_c = 0.05$ and the lower dashed line shows $\omega_c = 0.25$.

at lower multipoles and so the upper limits on ω_c are robust to the addition of these parameters. The CMB data have now reached the point where we have good constraints on the height of the first peak, as well as its location, and this is beginning to set interesting constraints on ω_c. The best fit value of $\Omega_m \approx 0.3$, derived from combining the CMB data with results from distant Type Ia supernovae (see figure 5) implies $\omega_c \approx 0.11$ for a Hubble constant of $h = 0.65$, consistent with the low values of ω_c favoured by the height of the first acoustic peak.

The left hand panel of figure 5 shows the marginalized likelihood for the CMB data in the Ω_Λ–Ω_m plane. The likelihood peaks along the line for spatially flat universes $\Omega_k = 0$ and it is interesting to compare with the equivalent figure in E99 to see how the new experimental results of the last year have caused the likelihood contours to narrow down around $\Omega_k = 0$. (See also Dodelson and Knox 1999 for a similar analysis using the latest CMB data). As is well known, the magnitude-redshift relation for distant Type Ia supernovae results in nearly orthogonal constraints in the Ω_Λ–Ω_m plane, so combining the supernovae and CMB data can break the geometrical degeneracy. The right hand panel in Figure 5 combines the CMB likelihood function derived here with the likelihood function of the supernovae sample of Perlmutter *et al.* (1999) as analysed in E99. The combined likelihood function is peaked at $\Omega_m \approx 0.3$ and $\Omega_\Lambda \approx 0.7$.

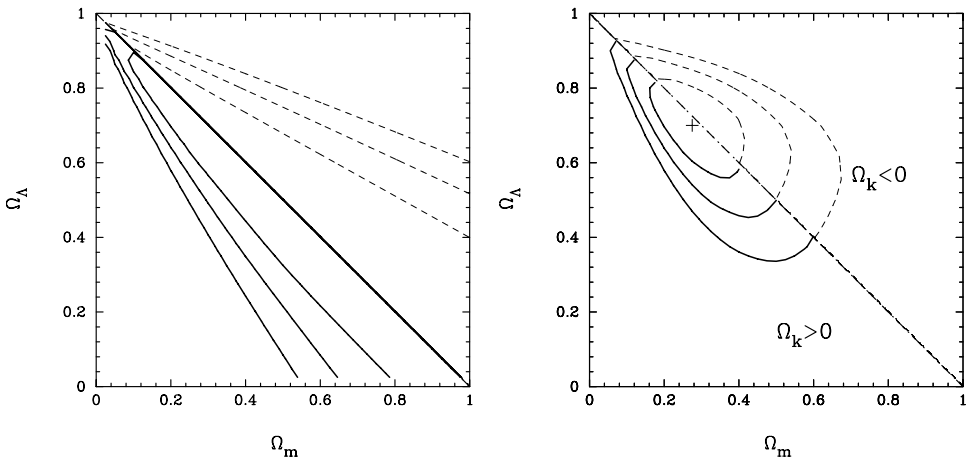

Figure 5. The figure to the left shows the 1, 2 and 3σ likelihood contours marginalized in the Ω_Λ and Ω_m plane from the observations plotted in figure 1. The figure to the right shows the CMB likelihood combined with the likelihood function for Type Ia supernovae of Permutter *et al.* (1999) as analyzed by E99. The dotted contours in both figures extend the CMBFAST (Seljak and Zaldarriaga 1996) computations into the closed universe domain using the approximate method described in E99.

It is remarkable how the CMB data and the supernovae data are homing in on a consistent set of cosmological parameters that are compatible with the simplest inflationary models and also with parameters inferred from a number of other observations (*e.g.* galaxy clustering, baryon content of clusters and dynamical estimates of the mean mass density, see Bahcall *et al.* 1999 for a review). It is also remarkable that the 'best fit' model requires a non-zero cosmological constant, a result that few cosmologists would have thought likely a few years ago.

The next few years will see a revolutionary increase in the volume and quality of CMB data. The results of the Boomerang Antarctic flight are awaited with great interest and should be of sufficient quality to render all previous analyses of cosmological parameters from the CMB obsolete. The polarization of the CMB has not yet been discovered, but a number of ground based and balloon borne experiments designed to detect polarization are under construction (Staggs, Gundersen and Church 1999). The MAP satellite, scheduled for launch in late 2000, will have polarization sensitivity and should determine the power spectrum C_ℓ accurately to about $\ell \sim 800$, defining the first three acoustic peaks. Further into the future, the Planck satellite, scheduled for launch in 2007, should determine the power spectrum to $\ell \gtrsim 2500$, provide sensitive polarization measurements and extremely accurate subtraction of foregrounds. Evidently, the era of precision

cosmology is upon us and the next decade should see a dramatic improvement in our knowledge of fundamental cosmological parameters and in our understanding of the origin of fluctuations in the early Universe.

References

1. Bahcall N., Ostriker J.P., Perlmutter S., Steinhardt P.J., (1999) The cosmic triangle: revealing the state of the Universe, *Science*, **284**, 1481-1488.
2. Bond J.R., (1996) Theory and Observations of the Cosmic Microwave Background Radiation, in Cosmology and large scale structure, eds Schaeffer R., Silk J., Spiro M., Zinn-Justin J., Elsevier Science, Amsterdam, 469-666.
3. Bond J.R., Jaffe A.H., Knox L., (1998) Estimating the power spectrum of the cosmic microwave background, *Phys. Rev. D*,**57**, 2117-2137.
4. Burles S., Tytler D. (1998) The deuterium abundance towards QSO 1009+2956, *ApJ*, **507**, 732-744.
5. Coble K., *et al.* (1999) Anisotropy in the cosmic microwave background at degree angular scales, *ApJ*, **519**, L5-L8.
6. Dodelson S., Knox S., (1999) Dark energy and the CMB. astro-ph/9909454.
7. Efstathiou G., Bond J.R., (1999) Cosmic confusion: degeneracies among cosmological parameters derived from measurements of microwave background anisotropies, *MNRAS*, **304**, 75-97.
8. Efstathiou G., Bridle S.L., Lasenby A.N., Hobson M.P., Ellis R.S., (1999) Constraints on Ω_Λ and Ω_m from distant Type Ia supernovae and cosmic microwave background anisotropies, *MNRAS*, **303**, L47-52.
9. Hu W., Sugiyama N., (1995) Towards understanding CMB anisotropies and their implications, *Phys. Rev. D*, **51**, 2599-2630.
10. Kamionkowski M, Kosowsky A., (1999) The cosmic microwave background and particle physics, *Ann. Rev. Nucl. Part. Sci.*, in press. astro-ph/9904108.
11. Hu W., White M., (1997) A CMB polarization primer, *New Astronomy*, **2**, 323-344.
12. Mauskopf P.D., *et al.* (1999) Measurement of a peak in the cosmic microwave background power spectrum from the North American test flight of Boomerang, *ApJ*, submitted. astro-ph/9911444.
13. Perlmutter S. *et al.* (1999) Measurement of omega and lambda from 42 high-redshift supernovae, *ApJ*, **517**, 565-586.
14. Peterson J.B. *et al.* (1999) First results from VIPER: detection of small-scale anisotropy at 40 GHz. *ApJ*, in press. astro-ph/9910503.
15. Rocha G., (1999) Constraints on the cosmological parameters using CMB observations, to appear in the proceedings of the 'Early Universe and Dark Matter Conference', DARK98, Heidelberg. astro-ph/9907312.
16. Sachs R.K., Wolfe A.M., (1967) Perturbations of a cosmological model and angular variations of the microwave background, *ApJ*, **147**, 73-90.
17. Seljak U., Zaldarriaga M., (1996) A line-of-sight integration approach to cosmic microwave background anisotropies, *ApJ*, **469**, 437-444.
18. Smoot G.F., (1992) Structure in the COBE differential microwave radiometer first-year maps, *ApJ*, **396**, L1-L5.
19. Staggs S.T., Gundersen J.O., Church S.E., (1999) CMB polarization experiments. astro-ph/9904062.
20. Tegmark M., Zaldarriaga M., (2000) Current cosmological constraints from a 10 parameter CMB analysis *ApJ*, submitted. astro-ph/0002091.
21. Zaldarriaga M., Spergel D.N., Seljak U., (1997) Microwave background constraints on cosmological parameters, *ApJ*, **488**, 1-13.